Polymer 52 (2011) 5817–5829

Contents lists available at SciVerse ScienceDirect

Polymer

journal homepage: www.elsevier.com/locate/polymer

Nanoporous poly(methyl methacrylate)-quantum dots nanocomposite fibers toward biomedical applications

Suying Wei [a,*], Jayanthi Sampathi [a], Zhanhu Guo [b], Narendhar Anumandla [a], Dan Rutman [b], Ashwini Kucknoor [c], Lauren James [c], Andrew Wang [d]

[a] Department of Chemistry and Biochemistry, Lamar University, Beaumont, TX 77710, USA
[b] Integrated Composites Laboratory (ICL), Dan F. Smith Department of Chemical Engineering, Lamar University, Beaumont, TX 77710, USA
[c] Department of Biology, Lamar University, Beaumont, TX 77710, USA
[d] Ocean NanoTech, LLC, 2143 Worth Ln., Springdale, AR 72764, USA

ARTICLE INFO

Article history:
Received 3 September 2011
Received in revised form
2 October 2011
Accepted 8 October 2011
Available online 18 October 2011

Keywords:
Nanoporous electrospun fibers
Fluorescence
Cell culture

ABSTRACT

In this work, poly(methyl methacrylate) (PMMA)-CdSe/ZnS quantum dots (QDs) nanocomposite fibers were fabricated via a simple electrospinning method. The parameters including concentration of PMMA, feed rate, applied voltage and working distance between the needle tip and the fiber collecting electrode were investigated and optimized to acquire large quantity, uniform and defect-free PMMA and its QD nanocomposite fibers. The surface morphology of the fibers was characterized by scanning electron microscopy (SEM), while the fluorescence emission characteristics of the polymer nanocomposite (PNC) fibers were analyzed with fluorescence microscopy. The thermal properties of the PMMA-QDs PNC fibers were explored by thermal gravimetric analysis (TGA) and differential scanning calorimetry (DSC). In comparison to the pristine PMMA fibers, the PNC fibers with only 0.1 wt% QD loading showed an improved thermal stability by 15 °C for the midpoint and onset degradation temperature. Surface chemical structure and functionalities were probed by a combination of attenuated total reflectance Fourier transform infrared (ATR-FTIR) spectroscopy and X-ray photoelectron spectroscopy (XPS). New vibration bands were observed in the PNC fibers in the ATR-FTIR spectra, while the binding energy for both high resolution C 1s and O 1s spectra in the PNC fibers showed an apparent shift toward lower field. Rheological studies revealed a pseudoplastic behavior of both pristine PMMA and PMMA-QDs solutions. Moreover, the formed nanoporous PMMA-QDs fiber media exhibited an excellent biocompatibility as evidenced by the model Chinese hamster ovary (CHO) cell culturing test. The CHO cells demonstrated good adhesion, growth and viability in the reported testing.

© 2011 Elsevier Ltd. All rights reserved.

1. Introduction

Poly (methyl methacrylate) (PMMA), a transparent thermoplastic, has been widely used in many commercial applications. For example, PMMA has been one of the most popular substrate materials in making polymer-based microfluidic devices to perform chemical and biological assays due to its excellent chemical, physical, biological, mechanical, optical and thermal properties [1–3]. In addition, PMMA is nondegradable and biocompatible which render it to be an excellent candidate in tissue engineering with typical applications such as fracture fixation, intraocular lenses and dentures [4,5]. PMMA has been traditionally used to fix bone fracture, and PMMA modified with N-methyl-pyrrolidone (NMP) has proved to be more mechanically amenable to bone repair and augment [6,7]. PMMA based hybrid structures have found great potentials in a variety of areas [8]. Development of PMMA based biocomposites such as PMMA-bovine serum albumin (BSA) nanoparticles (NPs) [9] may serve as a module for protein drug delivery, while cyclodextrin included PMMA nanostructures may be a potential choice of filtering media for organic pollutants remediation [10,11]. As quite a few PMMA based materials have received US Food and Drug Administration (U.S. FDA) approval and been applied in different areas since 1950s, it will be relatively easier to investigate PMMA based structures and explore the possibility to extend the laboratory results to clinical trial [12].

For the aforementioned tissue engineering application, it is very often desired to visualize the response of the surrounding cells and/or tissue to the implanted synthetic materials. Practically the

* Corresponding author. Tel.: +1 (409) 880 7654.
E-mail address: suying.wei@lamar.edu (S. Wei).

0032-3861/$ – see front matter © 2011 Elsevier Ltd. All rights reserved.
doi:10.1016/j.polymer.2011.10.012

semiconductor NPs, i.e. quantum dots (QDs) become one of the most favorite choices. CdSe/ZnS QDs are especially popular due to the uniqueness of core-shell structure and the less-toxicity of the shell, which can be made bioactive, with biomolecules such as protein or peptide coated on the shell surface. Water soluble QDs are novel tools in biomedical applications owing to their superior photoemission and photostability characteristics. Their unique fluorescence properties and diverse surface coatings with specific surface functionalities make it possible to use QDs to determine the cellular uptake pathways of small particles, tracking the cell imaging, immunohistochemistry and cancer cell targeting [13].

The electrospinning technology has been known for more than a century but real research work was boosted since the 1990s when Reneker and co-workers reintroduced this technique as a way to make submicron fibers [14,15]. Recently, electrospinning has

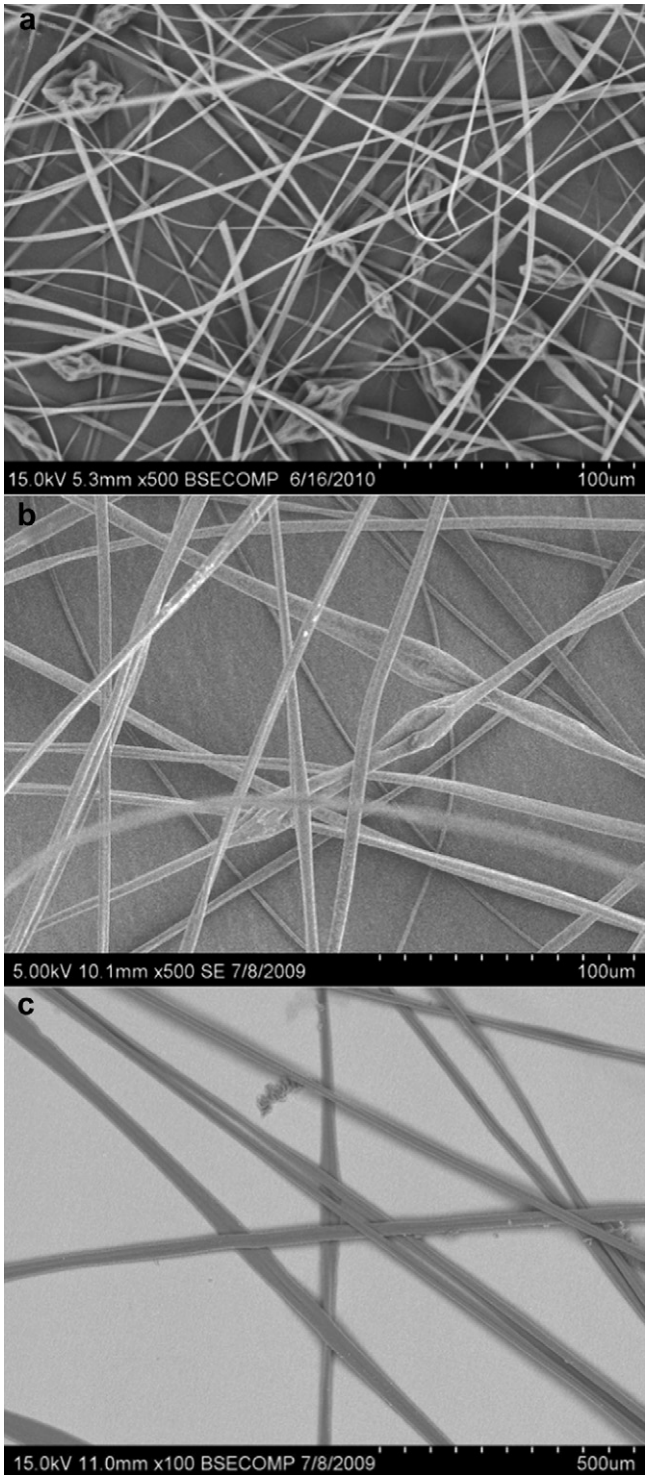

Fig. 1. SEM images of the pristine PMMA fibers electrospun from chloroform solution with a PMMA loading of (a) 10, (b) 12 and (c) 14 wt%. Other electrospinning operational parameters: 10 kV, 20 μL/min and 15 cm.

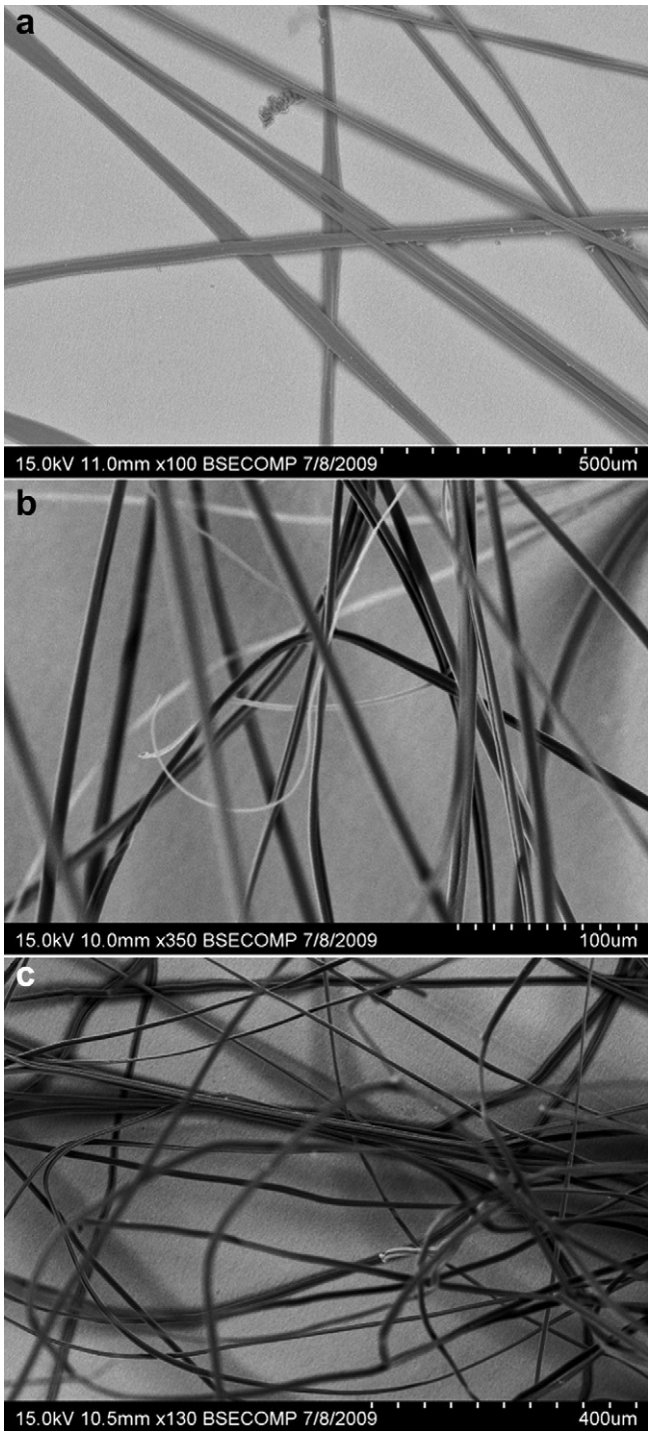

Fig. 2. SEM images of the pristine PMMA fibers electrospun at an applied voltage of (a) 10, (b) 20 and (c) 30 kV. Other electrospinning operational parameters: 20 μL/min, 15 cm and 14 wt% of PMMA.

become a versatile technique that enables the production of a variety of fibers bearing various desired functionalities from a wide range of materials, including polymers [16,17], polymer blends [18], sol–gels [19,20], composites [21–25], and ceramics [26,27]. Electrospun fibers have demonstrated some innovative applications, such as three-dimensional tissue scaffolds [28–30], energy devices and materials [31–34], sensors [35], and lightweight composites [21–25]. The incorporation of unique fillers into the fiber matrix either through inclusion in the pre-spinning solution or post-spinning treatment will integrate multi-functionalities and introduce unique synergistic properties into one targeted material unity and thus expand its corresponding applications.

Surface chemical functionality and topography are significant parameters that affect the performance of biomaterials in general,

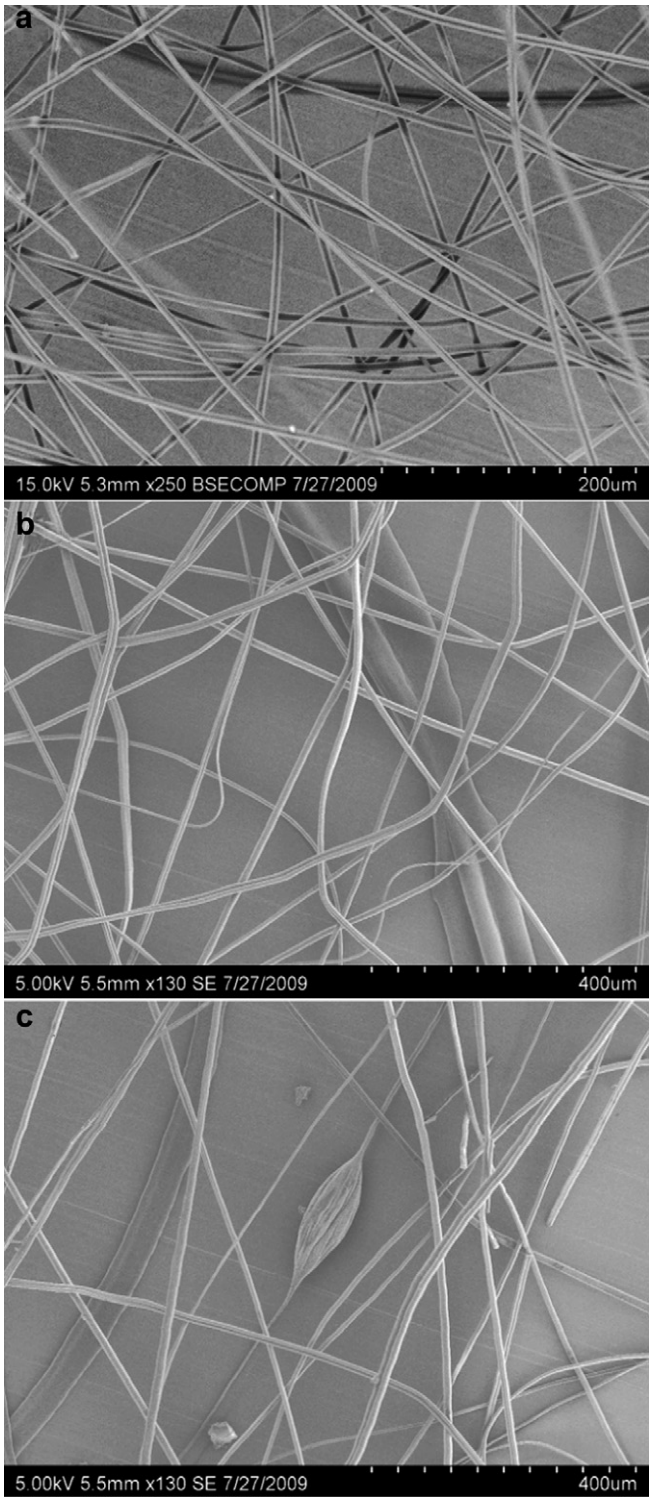

Fig. 3. SEM images of the pristine PMMA fibers electrospun with a working distance of (a) 10, (b) 15 and (c) 25 cm. Other electrospinning operational parameters are: feed rate 20 μL/min, polymer loading 14 wt% and voltage 20 kV.

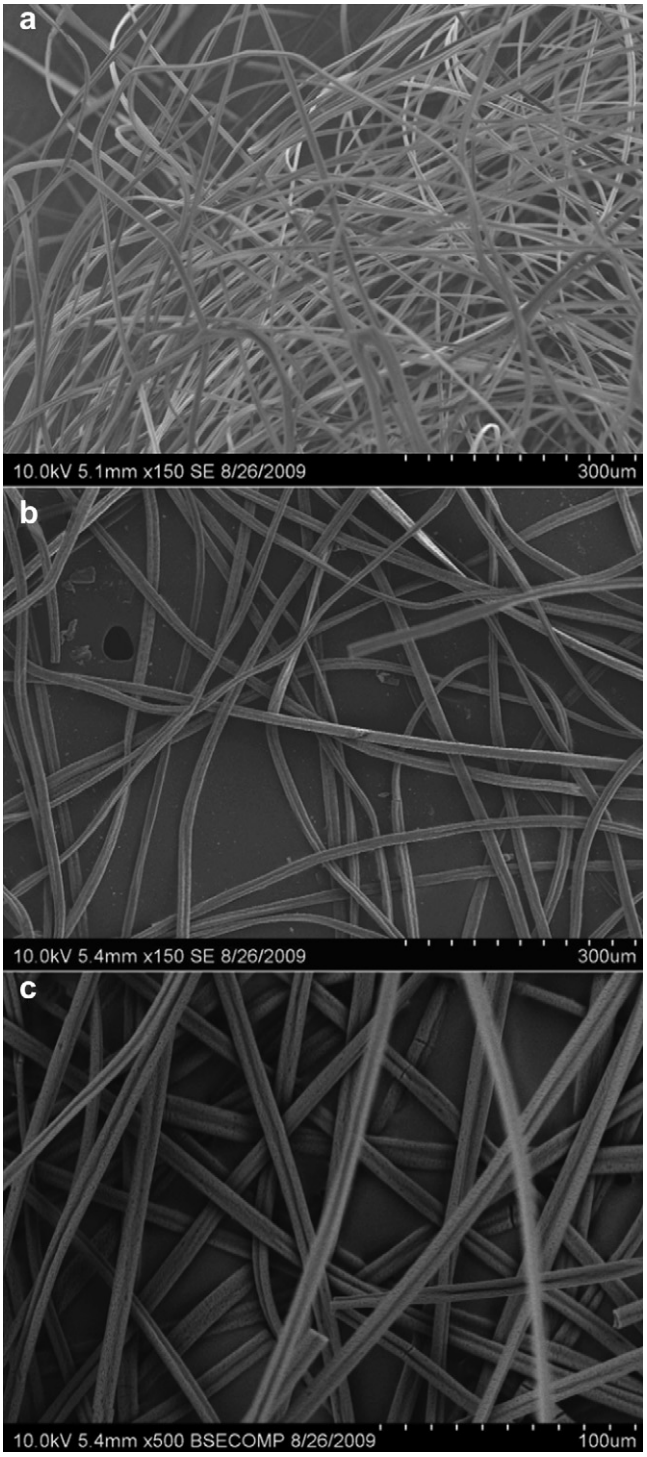

Fig. 4. SEM images of the pristine PMMA fibers electrospun at a flow rate of (a) 10, (b) 20 and (c) 30 μL/min. Other electrospinning operational parameters: 20 kV, 10 cm and PMMA loading of 14 wt%.

as they will determine the cell fate that comes in contact with the biomaterial. Furthermore, the mechanical and thermal performances also determine the fate of the polymer and polymer nanocomposites (PNCs) as biomaterials. However, very little work has been reported on a systematic exploration of the electrospinning production and characterization of PMMA and its QDs nanocomposite fibers. Here in this paper, pristine PMMA and its QDs composites fibers with different QD concentrations have been fabricated via a high voltage electrospinning process. By optimizing the process conditions (feed rate, applied electric voltage and working distance), bead-free and uniform fibers with complex nanopores were obtained at relatively lower concentrations of PMMA and 0.1 wt% QDs. The surface morphology and intermolecular interactions between the polymer backbone and the included QDs were characterized by scanning electron microscopy (SEM), attenuated total reflection Fourier transform infrared spectroscopy (ATR-FTIR), and X-ray photoelectron spectroscopy (XPS). The thermal stabilities and thermal behaviors of the PNC fibers were explored by thermal gravimetric analysis (TGA) and differential scanning calorimetry (DSC). The rheological behaviors of both polymer and its QD solutions were studied by rheometer. The Chinese hamster ovary (CHO) cells were used as a model epithelia cell type to explore the biocompatibility of the PMMA-QD fibers. The surface morphology effects on the cell adhesion, viability and growth characteristics were also investigated and detailed here.

2. Experimental

2.1. Materials

Poly(methyl methacrylate) (PMMA) (MW = 540,000) was purchased from Scientific Polymer Products and chloroform (99%) was purchased from Fisher Scientific. Core-shell CdSe/ZnS quantum dots (QDs; QSO-620-200) were kind gifts supplied by Ocean Nanotech, LLC. The QDs are supplied in chloroform with a concentration of 13.33 mg/mL. The surface group of the QDs is octadecylamine and

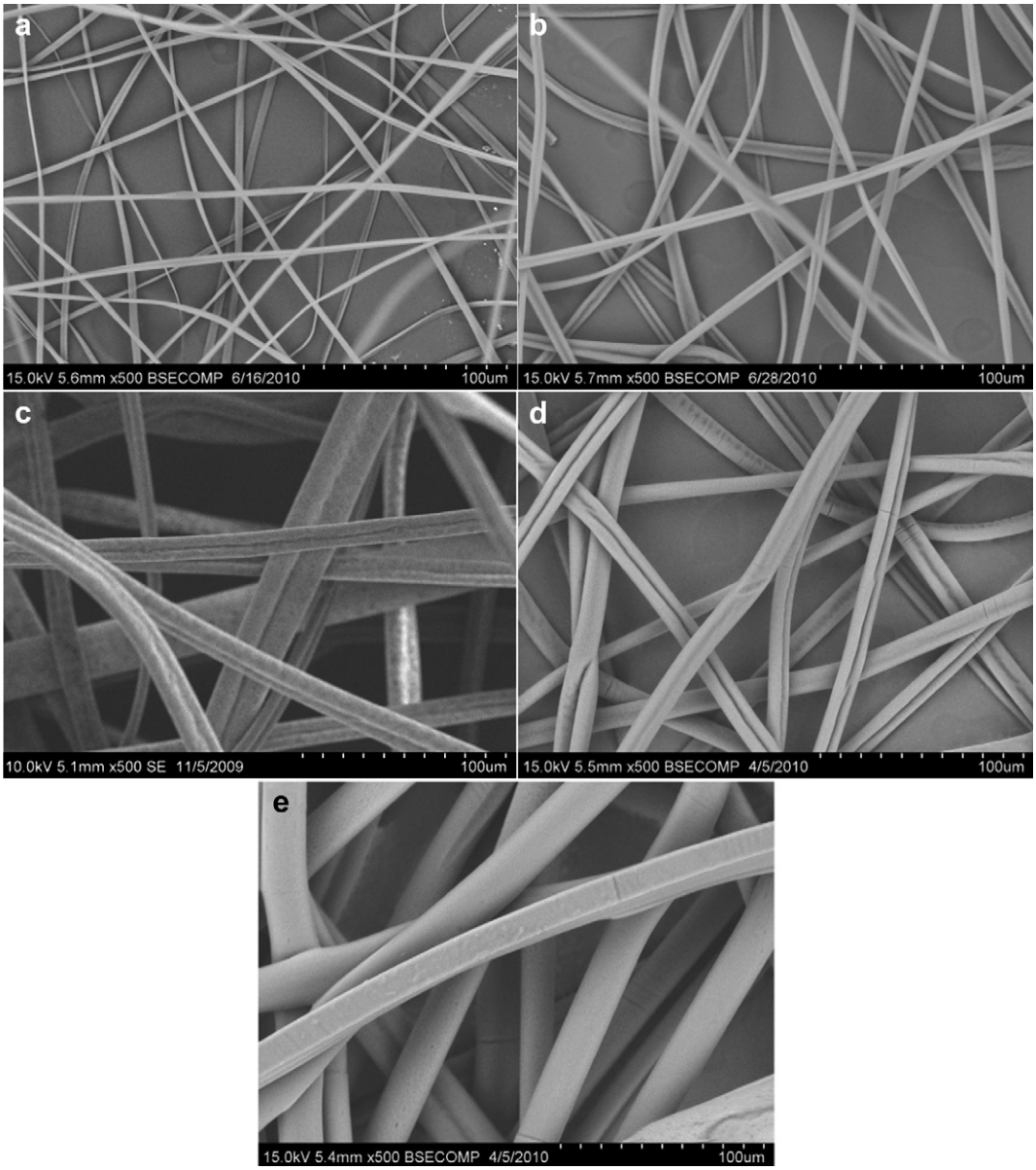

Fig. 5. SEM images of the PMMA-QD nanocomposite fibers electrospun with a PMMA loading of (a) 8, (b) 10, (c) 12, (d) 14 and (e) 22 wt%. The QD loading is 0.1 wt%. Other electrospinning operational parameters: 20 kV, 10 μL/min, and 15 cm.

the length of the surface ligand for the core/shell QDs is about 2 nm. The size of the QDs is about 10 nm, the full width half maximum (FWHM) of the used QDs is <35 nm, and the maximum fluorescence emission is at 620 nm. The Dulbecco's modified Eagle's medium (DMEM) and penicillin-streptomycin are purchased from Invitrogen, while the 10% fetal bovine serum (FBS) is from Atlanta Biologicals. Trypan blue and methylene blue are from Sigma while the 8-well chambered slides are purchased from BD Biosciences. All the materials were used as received without any further treatment.

2.2. Electrospinning of PMMA and PMMA-QDs nanocomposite fibers

The polymer chloroform solutions with different polymer concentrations of 10, 12 and 14 wt% were prepared by dissolving PMMA pellets in chloroform. The PMMA fibers were fabricated by the electrospinning process. A 5-mL syringe with an inner diameter of 0.6 mm was used for the electrospinning facilitated by a syringe pump (NE-300) from New Era Pump Systems, Inc. and a high voltage power supply (Model No. ES3UP-5w/DAM) purchased from Gamma High Voltage Research. The PMMA-QDs nanocomposite fibers were fabricated from the PMMA solutions with a PMMA concentration of 8, 10, 12, 18 and 22 wt% and QD concentration of 0.04, 0.06, 0.08 and 0.1 wt% (against the neat polymer). Other electrospinning parameters including the feed rate, applied high voltage and distance from the receiving substrate to the syringe needle tip were explored and optimized to obtain desired fibers.

2.3. Characterization of electrospun PMMA and PMMA-QDs nanocomposite fibers

Surface morphology of the electrospun fibers was characterized by scanning electron microscopy (Hitachi S-3400 SEM), while the molecular interactions between the polymer and the QDs were probed via surface analysis techniques including attenuated total reflectance Fourier transform infrared spectroscopy (ATR-FTIR;

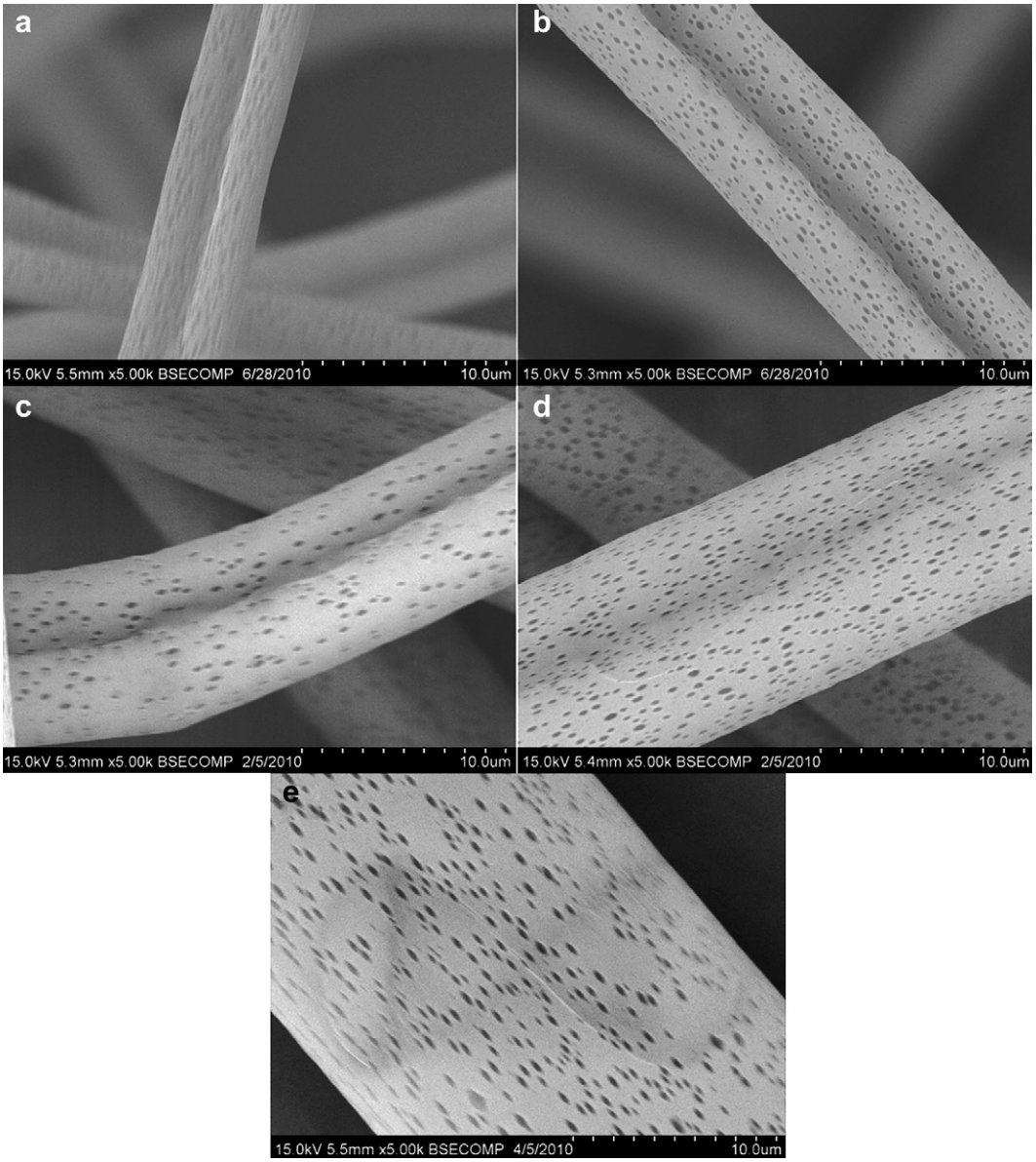

Fig. 6. High resolution SEM images of PMMA-QD nanocomposite fibers electrospun from solutions with a PMMA loading of (a) 8, (b) 10, (c) 12, (d) 14 and (e) 22 wt%, respectively. The QD loading is 0.1 wt%. Other electrospinning operational parameters: 20 kV, 10 μL/min, and 15 cm.

Bruker Alpha) and X-ray photoelectron spectroscopy (XPS). XPS measurements were carried out by a Kratos Axis Ultra Imaging X-ray photoelectron spectrometer with pass energy of 40 eV for high resolution spectra. The thermal stability was studied by thermo gravimetric analysis (TGA; TA instruments Q-500) from room temperature to 700 °C at a heating rate of 10 °C/min under 60 mL/min air atmosphere. Differential scanning calorimetry (DSC; TA instruments Q20) analysis was done under the nitrogen purge at a flow rate of 50 mL/min. Each sample was first heated from room temperature to 240 °C with a heating rate of 10 °C/min to remove thermal history, followed by cooling down to 40 °C at a rate of 10 °C/min to record re-crystallization temperature, and then reheating to 240 °C at the same rate to determine the glass transition temperature and melt temperature. The sample weight was normally between 6 and 9 mg. The glass transition temperature is recorded according to the most commonly accepted way in literature, i.e., the midpoint of the heat flow (capacity) step transition between the glass and rubbery states. The rheological behaviors of solution samples were determined using TA instruments AR2000ex Rheometer in the shear rate range of 1–1000 rad/s at 25 °C. The optical properties of the PMMA-QDs composite fibers were studied by measuring UV–vis absorption (Varian Spectra AA 220) and the fluorescence emission (Varian Cary Eclipse Fluorescence Spectrophotometer). The unique fluorescence images of the composite fibers were demonstrated by fluorescence microscopy (Olympus BX41 Epifluorescence microscope equipped with Olympus DP-71 camera and cellsem software). The time exposure used was 20.0 ms and magnification was 10×.

2.4. The Chinese hamster ovary (CHO) cell biocompatibility study

CHO cells obtained from American Type Culture Collection (ATCC) were cultured under standard conditions, with DMEM containing 10% FBS and 100 U/mL penicillin-streptomycin in a 37 °C tissue culture incubator with 5% CO_2. CHO cells were trypsinized upon reaching confluence, enumerated using hemocytometer. For co-culture, fibers were sterilized by incubating in 70% ethanol for 2 h, followed by 20 min exposure to UV light [35]. Fibers were then washed with plain DMEM and air dried before immobilizing onto wells on 8-well chambered slides (BD Biosciences). Each well had equal amounts of fibers, and CHO cells were introduced into these wells at 1×10^4 cells/well. The slides were incubated for 24, 48 and 72 h.

2.4.1. Cell viability assay

Trypan blue dye exclusion assay [36] was used to determine the viability of the CHO cells, following incubation with the fibers. Following incubation for different time periods, the culture medium was removed and the cells were stained with 0.2% Trypan Blue for 10 min. The dye was washed off and cells were trypsinized and counted under microscope using hemocytometer to detect any dead cells. Microscopic observation of the CHO cells growth pattern: CHO cells grown on chambered slides co-cultured with electrospun fibers were stained with 0.25% methylene blue for 20 min. Stain was washed with 1× phosphate buffered saline (PBS) and the slides were viewed under BX41 Olympus microscope, and images were captured using CellSens software.

3. Results and discussion

3.1. Morphological analysis of electrospun PMMA fibers

To obtain fine, uniform and beads free fibers in a relatively large quantity necessary toward the desired applications, the electrospinning parameters were explored theoretically and experimentally [37]. The optimum set of the operational parameters were

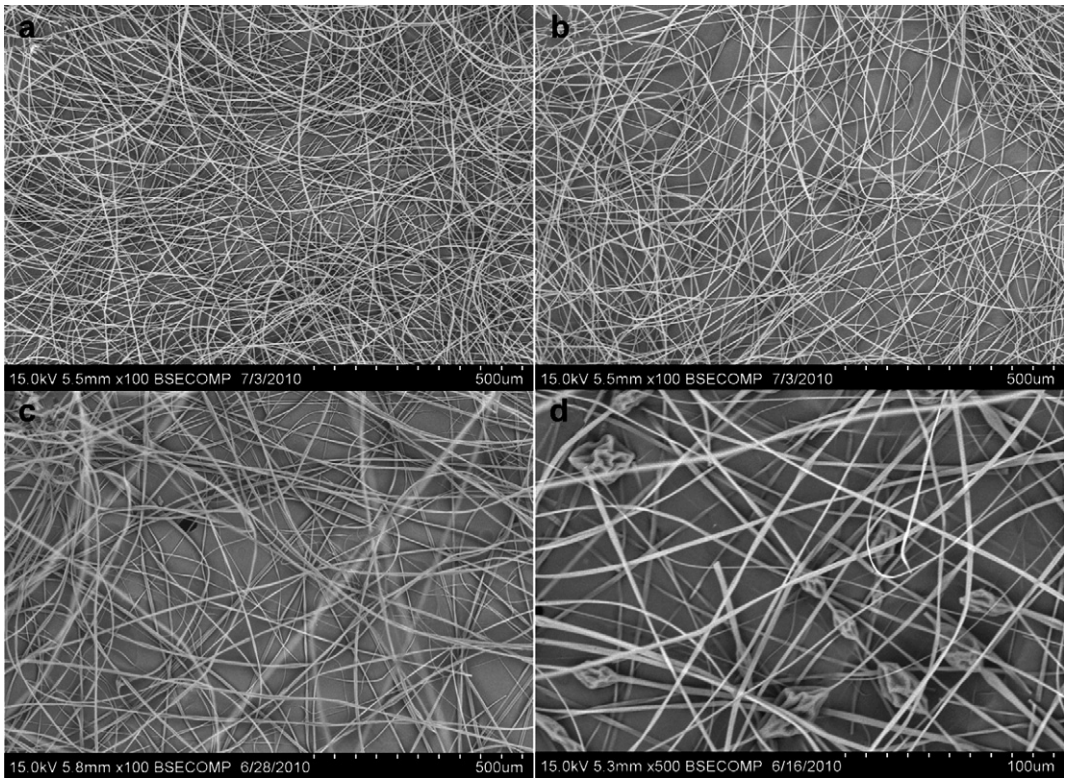

Fig. 7. SEM images of the PMMA nanocomposite fibers electrospun at a distance of (a) 5, (b) 10, (c) 15 and (d) 25 cm. Other electrospinning operational parameters: 20 kV, 2 μL/min, QD loading of 0.1 wt% and the PMMA loading of 8 wt%.

obtained by studying the morphological features with SEM. In general, the PMMA fibers electrospun from the chloroform solution are ribbon like with a range of different sized nanopores along the fiber surface, which is probably due to the fast evaporation of solvent and the cooling effect on the fiber surface during the electrospinning process, causing the so-called thermally induced phase separation (TIPS), thus pores formation on the fiber surfaces [38]. Fig. 1 shows the SEM microstructures of the pristine PMMA fibers electrospun from chloroform solutions with a PMMA loading of 10, 12 and 14 wt%, respectively. The feed rate, working distance and applied voltage are maintained constant at 10 kV, 20 μL/min and 15 cm, respectively. Defect-free fibers are observed with increasing the PMMA loading in chloroform. The formation of beads is the result of surface tension of the solution, which is related to the polymer entanglements, at higher polymer loading, i.e. higher viscosity, the solvent molecules get distributed over the entangled polymer molecules thus avoiding beads formation. The polymer loading is observed to have a significant effect on the fiber diameter. The diameter is 2.38 ± 0.36, 5.40 ± 0.93 and 22.55 ± 4.45 μm for the fibers electrospun from the polymer solution with a PMMA loading of 10, 12 and 14%, respectively. Optimization of the applied voltage was demonstrated in Fig. 2, in which SEM images of the pristine PMMA fibers prepared at 10, 20 and 30 kV with other operational parameters fixed at 20 μL/min feed rate, 15 cm working distance and 14 wt% concentration of PMMA. In most cases, a higher voltage will lead to greater stretching of the solution due to the greater columbic forces and thus causes a reduced diameter of the fibers. A longer flight time will allow more time for the fibers to be stretched and elongated before they are deposited on the collection plate. The reduced acceleration of the jet and the weaker electric field due to lower voltage increases the flight time of the electrospinning jet, which favors the formation of finer fibers. In Fig. 2, the diameter (23.21 ± 7.48 μm) of fibers produced from 10 kV is much bigger than that (7.02 ± 1.39 μm) from 20 kV, while the SEM image of PMMA fibers from 30 kV shows an increased diameter

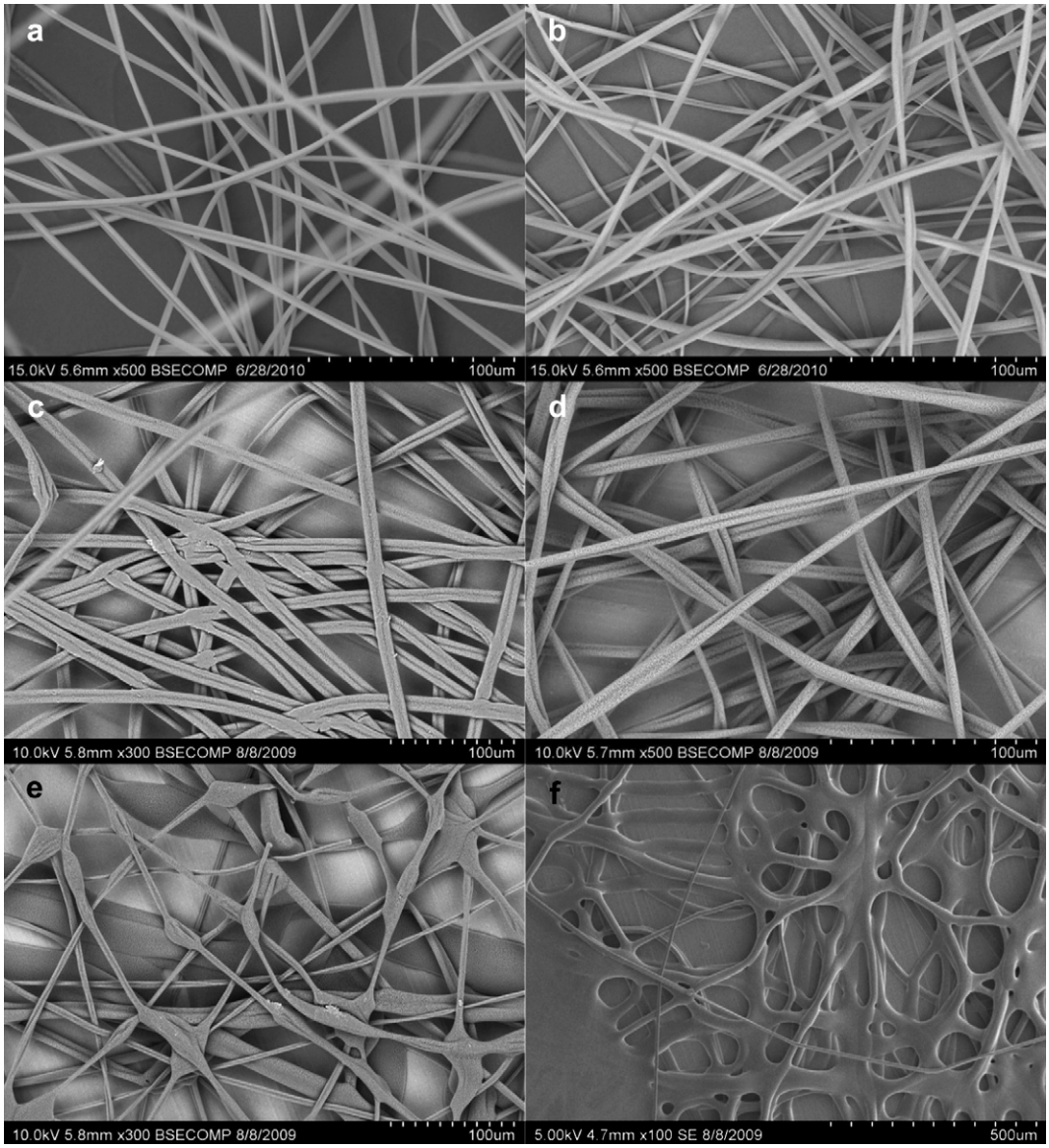

Fig. 8. SEM images of PMMA nanocomposite fibers electrospun at a feed rate of (a) 2, (b) 10, (c) 30, (d) 40, (e) 50 and (f) 70 μL/min. Other electrospinning operational parameters: 20 kV and 10 cm. The QD loading is 0.1 wt% and the PMMA loading is 8 wt%.

(9.43 ± 3.10 μm) again and also some broken fibers are observed. Therefore, 20 kV is used as the optimum applied voltage in this case while the mass percentage was kept at 14 wt%. Fig. 3 shows the variation in fibers formation when working distance is varied. The other parameters were maintained constant with an applied constant voltage of 20 kV, PMMA concentration at 14 wt% and a feed rate of 20 μL/min. At an increased distance, thicker fibers (11.02 ± 1.85 μm) were observed at 15 cm compared to those (6.30 ± 1.00 μm) electrospun at 10 cm and beads were also observed at longer distances due to the decrease in electric field strength and less stretching of the fibers. Slightly thicker fibers (11.32 ± 2.43 μm) are observed while electrospun at 25 cm. From this set of study 10 cm was adopted for later preparation of PMMA fibers. Fig. 4 shows the effect of feed rate on electrospun PMMA fibers. As the feed rate was increased, more uniform and relatively shorter fibers were produced as the broken ends started to appear at higher feed rate with 14 wt% PMMA concentration, 10 cm distance and 20 kV applied voltage. No beads were observed along the fibers due to the varied feed rate. The diameter is 7.53 ± 2.48, 14.11 ± 2.51 and 7.98 ± 1.27 μm for the fibers electrospun at a flow rate of 10, 20 and 30 μL/min, respectively. In summary, the optimum set of the electrospinning parameters from the series of studies is 14 wt%, 20 kV, 10 cm and 20 μL/min, and the produced fibers have a diameter from 10 to 15 μm with nanopores between 100 and 250 nm.

3.2. PMMA-QDs electrospun nanocomposite fibers

PMMA-QDs composite solutions were electrospun and optimized to obtain defect-free fibers. Figs. 5–8 show the SEM images of each step of manipulation resulted from different operational parameters. The electrospun nanocomposite fibers were made from PMMA loading of 8, 10, 12, 14 and 22 wt% with 0.1 wt% QDs in chloroform. The other parameters were maintained at 10 μL/min feed rate, 20 kV applied voltage and 15 cm working distance. As the PMMA concentration of the solution increases, the diameter of the fibers increases, Figs. 5 and 6. The diameter of the fibers obtained from 8 wt% PMMA-QDs nanocomposite fibers is around 5 μm. Fig. 7 shows the working distance effect on the electrospun PMMA-QDs nanocomposite fibers at 5, 10, 15 and 25 cm while keeping constant 8 wt% PMMA-0.1 wt% QDs, 2 μL/min feed rate and 20 kV applied voltage. An increase in the distance is observed to result in less uniform fibers, and even beads are observed in fibers electrospun at too large distance. Fig. 8 shows the effect of feed rate on the electrospun PNC fibers fabricated at 8 wt% PMMA-0.1 wt% QDs, 10 cm distance and 20 kV applied voltage. Diameter of the fibers starts to increase as the feed rate increases and also the web like structures are observed with increasing the feed rate further. Fine, uniform and individual fibers are produced at 2 and 10 μL/min feed rate. The diameter of the fibers obtained from the above parameters is 5–20 μm.

3.3. Surface chemical structure and functionality analysis

Fig. 9 shows the ATR-FTIR spectra of the electrospun fibers prepared from 8 wt% pristine PMMA, 8 wt% PMMA with 0.06 wt% QDs, 8 wt% PMMA with 0.08 wt% QDs and 8 wt% PMMA with 0.1 wt% QDs. The peak at 2950 cm^{-1}, which is not observed in the pristine PMMA fibers while present in all the composite fibers [1], corresponds to the C–H stretching arising from the organic coating layer on the QD surface. As the weight percentage of QDs increases, the peak becomes more intense. The peak observed at 1145 cm^{-1} is attributed to the H–C–H stretching, and the 1437cm^{-1} peak is from the CH_3 bending. The peak at 1725 cm^{-1} is due to the C=O stretching and the peaks at 991 cm^{-1} and

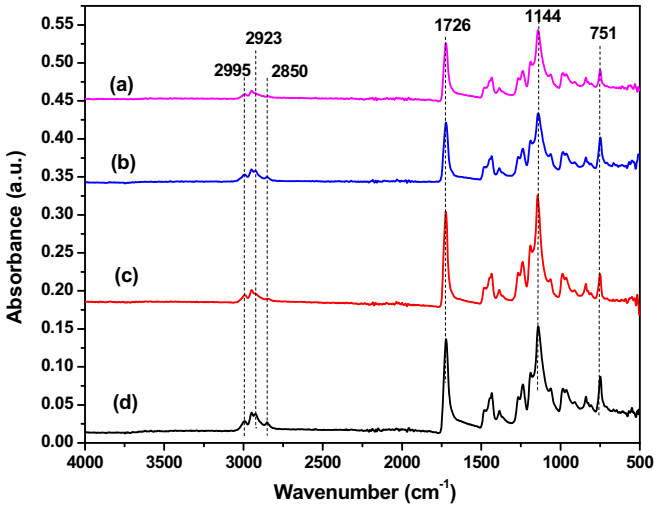

Fig. 9. ATR-FTIR spectra of (a) pure PMMA fibers electrospun from 8 wt% PMMA solution and PMMA-QDs nanocomposite fibers from 8 wt% PMMA solutions and a QD loading of (b) 0.06, (c) 0.08 and (d) 0.1%, respectively.

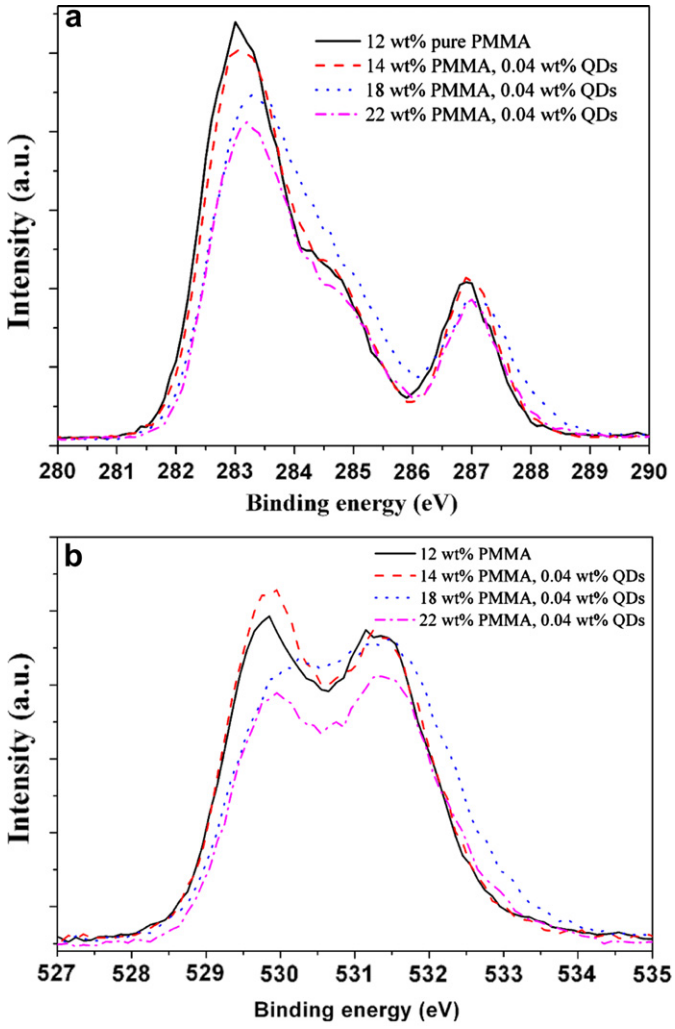

Fig. 10. XPS high resolution (a) C 1s and (b) O 1s spectra of electrospun pristine PMMA and its QD nanocomposite fibers.

751 cm^{-1} correspond to C–H out of plane bending, and the peaks are intensified with the addition of the QDs. The peak at 553 cm^{-1} corresponds to the sulfone stretching which is not observed in the 8 wt% PMMA fibers without QDs. By the addition of QDs to PMMA polymer, the peaks get intensified as the weight percentage of the QDs is increased. Two distinct peaks are observed in the PMMA/QDs liquid sample (spectrum not shown), one at 3026 cm^{-1} and the other at 1215 cm^{-1}. The band at 3026 cm^{-1} is due to the N–H stretch of amines and 1215 cm^{-1} corresponds to the C–N stretch of aliphatic amines due to the octadecylamine surface coating on the QDs [39]. Neither peak is visible in the ATR-FTIR nanocomposite fiber spectra due to the rigidity of the solid state materials.

As a powerful surface analysis technique, XPS provides information on the elemental composition and oxidation states of the element within 10 nm range of the surface. Fig. 10 shows the C 1s and O 1s high resolution spectra of pristine PMMA and PMMA-QDs PNC fibers with different PMMA mass percentage. Both C 1s and O 1s high resolution spectra are observed shifted about 0.3 eV toward higher binding energy in the samples with higher mass percentage of PMMA, i.e., 18 and 22 wt%, which is attributed to the organic coating layer on the surface of QDs. For the PMMA-QDs composite fibers with higher loading of QDs showed larger energy shift compared to that of pristine PMMA fibers.

3.4. Thermal gravimetric analysis (TGA) and differential scanning calorimetry (DSC)

In order to study the thermal properties of neat PMMA and its QDs nanocomposite fibers, both thermal gravimetric analysis (TGA) and differential scanning calorimetry (DSC) were performed. Fig. 11(a) shows the TGA curves of the samples. Both PMMA and PMMA-QDs exhibit two distinct slopes: the first weight loss from room temperature to 265 °C results from the evaporation of residual moisture and solvent, and the removal of low molecular weight molecules, while the second weight loss which plateaus around 440 °C is due to the complete decomposition of PMMA [33]. In comparison, the PMMA-QDs nanocomposite fibers show an improved thermal stability at both TGA $T_{0.5}$ (50% weight loss region in the TGA thermogram) and TGA $T_{0.1}$ (onset degradation temperature i.e., 10% weight loss region in the TGA thermogram) as reported previously [40]; PMMA-QDs nanocomposite fibers with 12 wt% PMMA loading show an increment of 15 °C for both onset and midpoint regions, PMMA-QDs nanocomposite fibers with 10 wt% PMMA loading show increased 5 °C at midpoint while 12 °C at the onset point, and PMMA-QDs nanocomposite fibers with 8 wt% PMMA loading are improved 8 °C at midpoint but only 1 °C at the onset. This enhanced thermal stability is significant for only 0.1 wt% QD

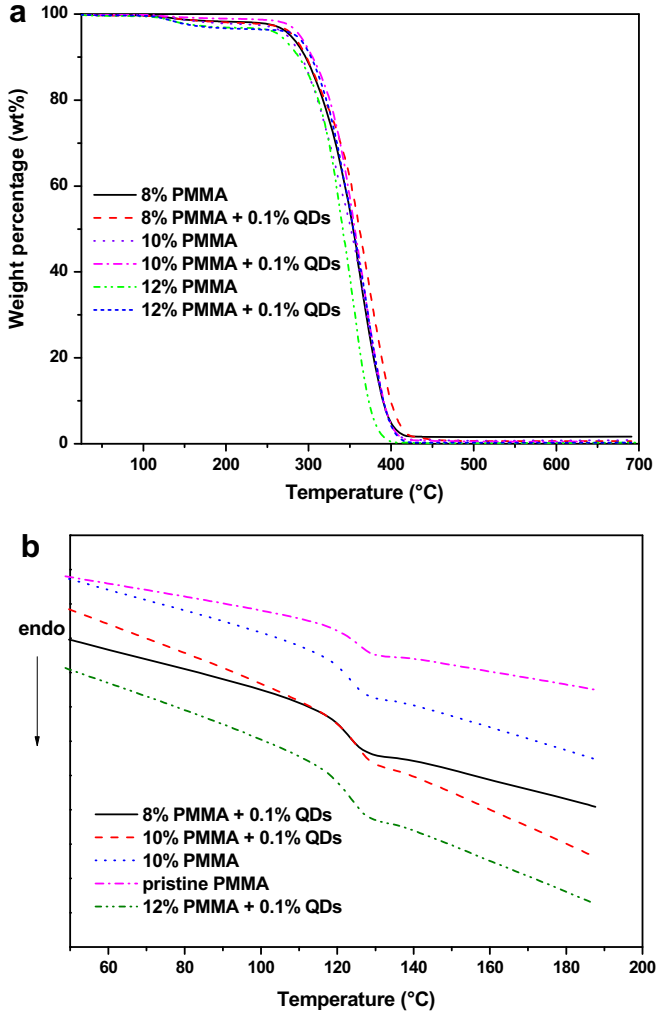

Fig. 11. (a) TGA curves of the pristine PMMA and its nanocomposite fibers; and (b) DSC thermograms of pristine PMMA and its nanocomposite fibers.

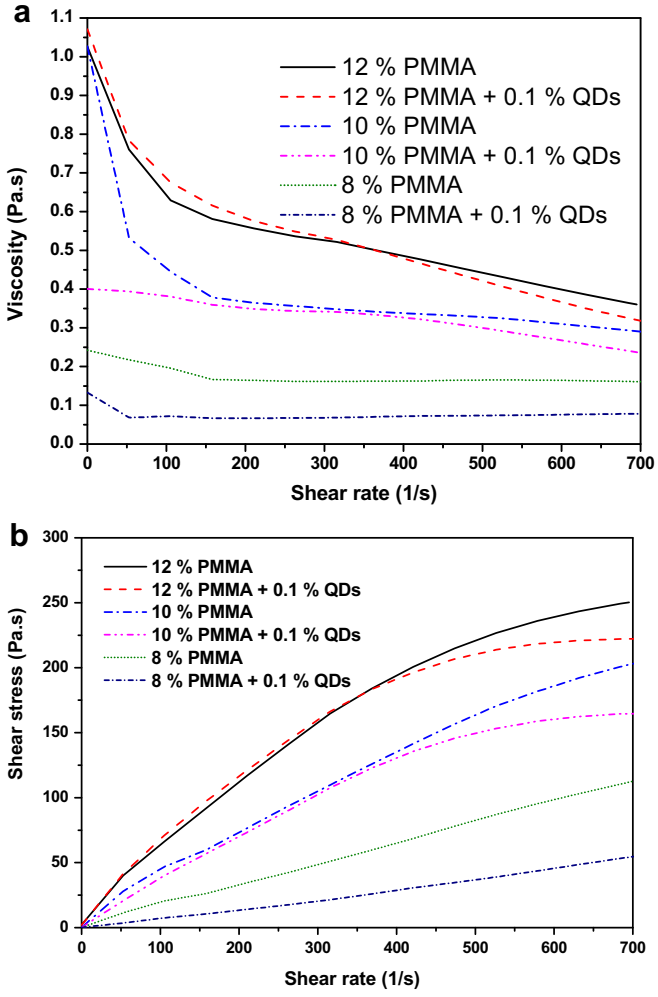

Fig. 12. (a)Viscosity and (b) shear stress vs. shear rate of PMMA and PMMA-QDs solutions.

loading in the PNC fibers. It may be due to the free radical absorption by the QDs during the thermal decomposition of PMMA and hence retards the polymer mobility, similar to other reported polymer nanocomposite systems [41–44].

The phase behavior of the PNCs affected by inclusion of a small fraction of QDs was exploited in a differential scanning calorimetry (DSC) by checking the glass transition temperature (T_g) change. DSC was performed under nitrogen purge in which two heating cycles and one cooling cycle were used so that the previous heating history was removed during the first heating cycle, while the second heating cycle and the cooling cycle were used for data analysis. From Fig. 11(b), the as-received pristine PMMA showed a T_g of 124 °C, while PMMA and its QDs nanocomposite fibers showed a relatively lower T_g of 121 and 119 °C respectively. The

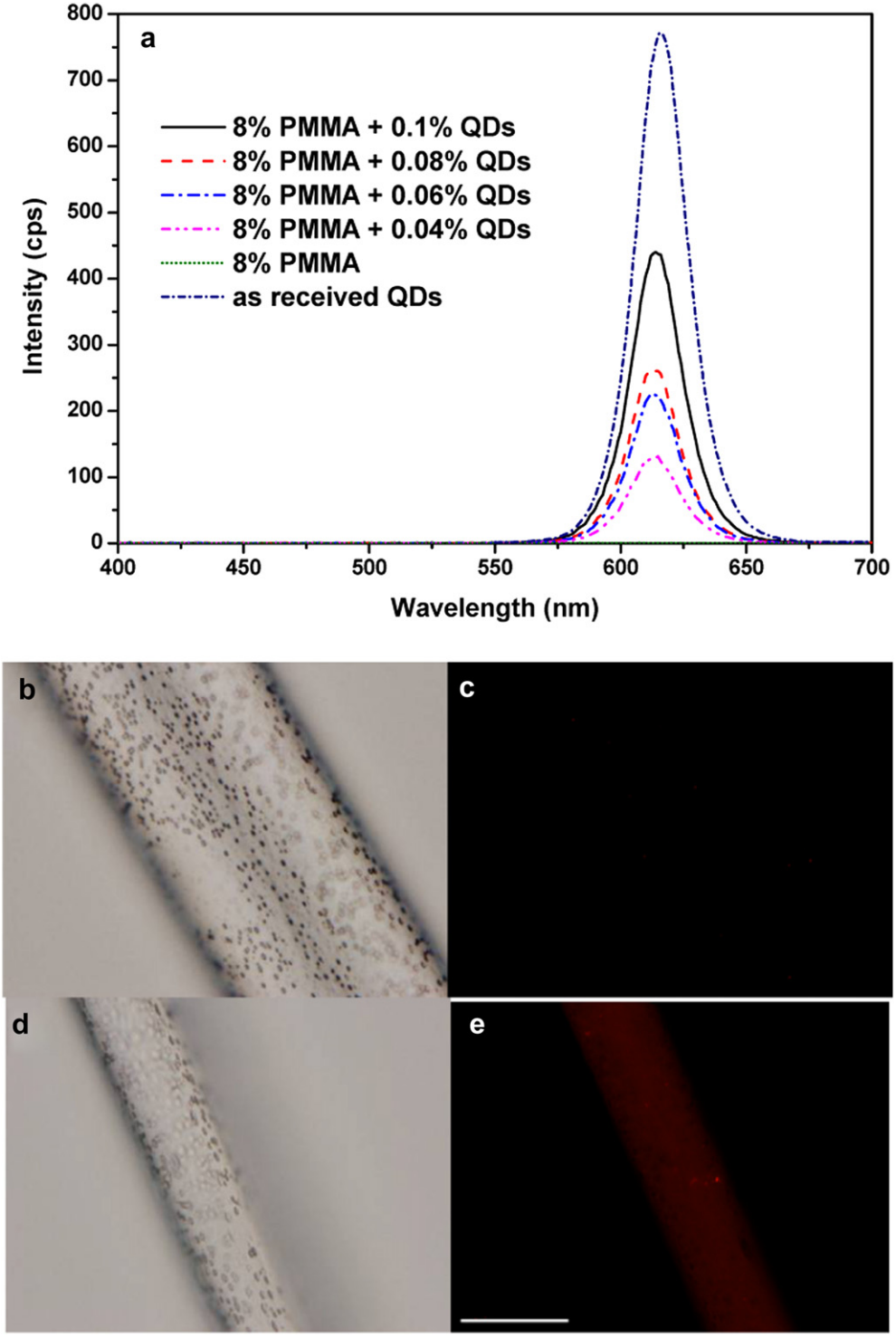

Fig. 13. (a) Fluorescence emission spectra of PMMA and PMMA-QDs solutions; fluorescence microscopic images of pristine PMMA fibers in (b) bright field and (c) dark field; and PMMA-QD nanocomposite fibers in (d) bright field and (e) dark field. (scale bar: 5 μm).

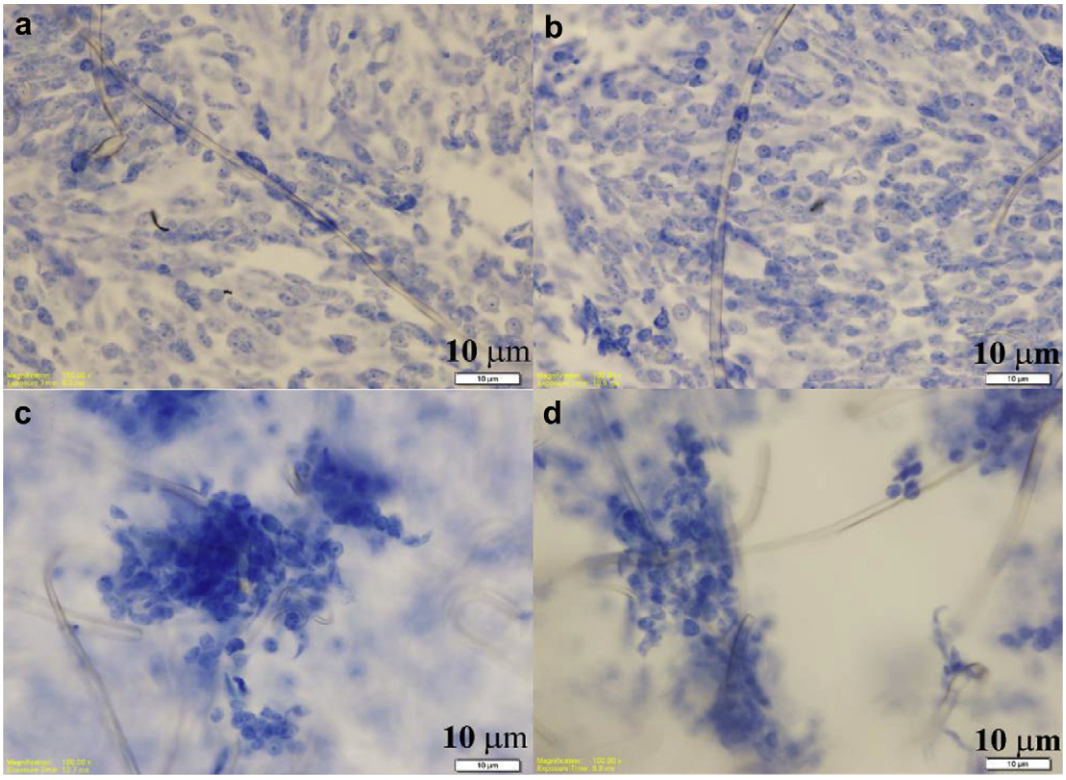

Fig. 14. (a) Methylene blue stained CHO cells after 24 h of seeding in the presence of fibers (8 wt% PMMA with 0.1 wt% QDs); (b) Cells at 48 h of growth; (c) and (d) show the cell growth on fibers that were separated from the previous well with cells at 48 h growth and resuspended with fresh medium on a new well for another 24 h, to determine if the cells that were attached to the fibers were able to grow and proliferate further.

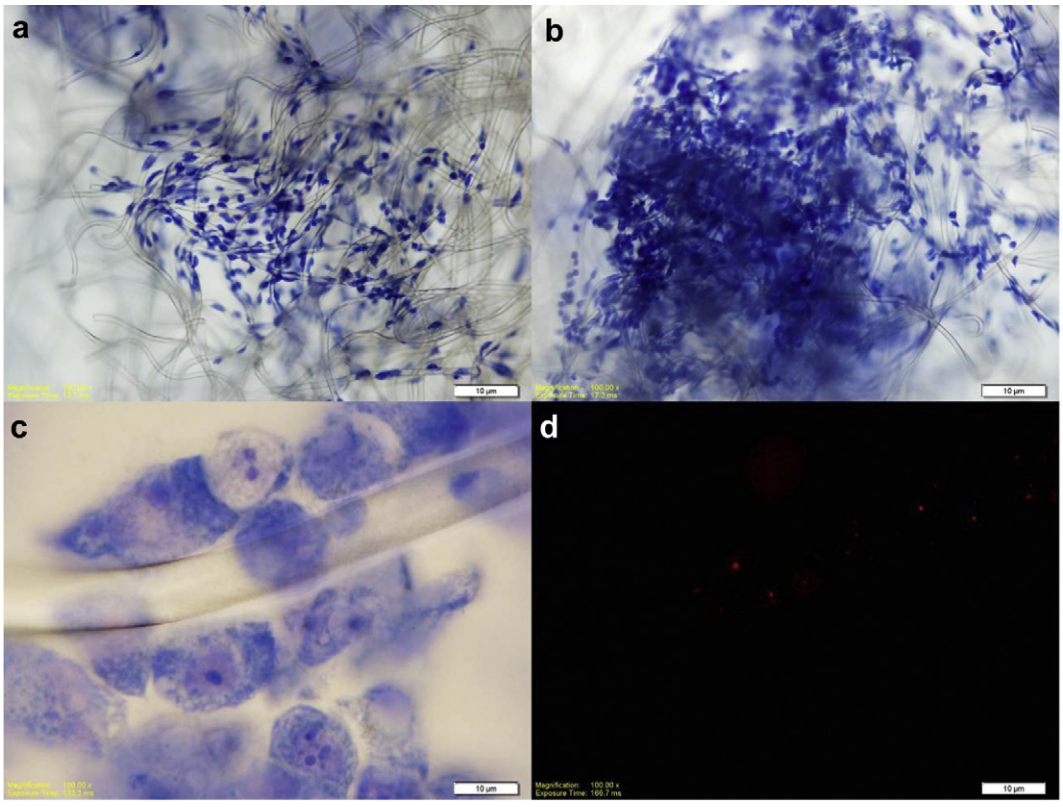

Fig. 15. (a) The growth of CHO cells after 24 h on fibers (12 wt% PMMA with 0.1 wt% QDs); (b) growth of cells after 48 h; (c) The cell shape and morphology after 48 h growth under higher magnification and (d) The fluorescence of quantum dots on the fiber in (c). Scale bar: 10 μm.

lower T_g is attributed to the interaction between the QDs and the PMMA backbone.

3.5. Solution rheological study of the pristine PMMA and PMMA/QD

Fig. 12(a and b) shows the viscosity and shear stress as a function of the shear rate for the PMMA and PMMA/QD solutions. The viscosity increases with increasing the PMMA loading, Fig. 12(a). With the addition of QDs to the PMMA, the viscosity decreases when compared with that of the neat PMMA solution. The shear stress versus shear rate plot does not follow a linear relationship, Fig. 12(b), in the PMMA and PMMA/QD solutions, which is the characteristic of Newtonian fluids. The curve obtained shows the pseudoplastic nature of the polymer solution, in which viscosity decreases with increased stress [45–49].

3.6. Fluorescence analysis of the PMMA-QDs nanocomposite fibers

Fig. 13(a) shows the fluorescence emission profiles of the pristine PMMA and PMMA/QDs in chloroform. Fig. 13(b–e) shows the electrospun pristine PMMA and PMMA-QDs nanocomposite fibers. A strong fluorescence peak at 614 nm, which resembles that of the as-received QDs solution in the same chloroform solvent, is observed. As the concentration of the QDs increases in the PMMA/QDs solution, the intensity of fluorescence peak increases, Fig. 13(a). Pristine PMMA is transparent in the visible and near infrared range as expected, and shows no fluorescence emission when excited. The pristine PMMA fibers show no background fluorescence emission, Fig. 13(c), while the PMMA-QDs nanocomposite fibers show distinct red color along the fiber uniformly Fig. 13(e).

3.7. Cell growth and viability study on the PMMA-QDs nanocomposite fibers

Figs. 14 and 15 summarized the typical cell culture data in the presence of two sets of PMMA-QDs nanocomposite fibers; fibers in Fig. 14 has an 8 wt% PMMA loading plus 0.1 wt% QDs inclusion while fibers in Fig. 15 has a 12 wt% PMMA loading and 0.1 wt% QDs inclusion. In general, the two sets of nanocomposite fibers show similar effects on the CHO cell behavior over the span of culture time: at the beginning, the cells tended to avoid immediate contact with the fiber, but when the culture time was continued further the cells started to adhere to the fibers and grew surrounding the fibers. It indicated that the CHO cells adjusted themselves over time and showed good adhesion and growth in the presence of the PMMA-QDs nanocomposite fibers. Cell proliferation assays showed that different fibers used for co-culture with CHO cells supported the growth and proliferation of CHO cells very well as compared with the control cell growth. Cell growth measured by the increased cell numbers was not significantly different between the control cells and the cells that were grown in the presence of the fibers. Microscopic observations using methylene blue stained cells showed no difference in the cell morphology and proliferation. Cells were growing on and around the individual fibers and over prolonged growth period, there was formation of confluent monolayers as seen on control cells without fibers. Cell viability assay using Tryphan blue dye exclusion showed that there was no cell death due to the chemical composition of the fibers (data not shown).

4. Conclusion

Electrospun PMMA-QDs nanocomposite fibers were successfully prepared by incorporating QDs in the pre-electrospinning polymer solution. Monitored by SEM morphological analysis and the theoretical guidance, large quantity of fine, uniform and defect-free fibers were obtained at low concentrations of PMMA and 0.1 wt % QDs. Surface analysis by the ATR-FTIR and XPS techniques indicate that the QDs are incorporated onto the electrospun polymer fibers, which shifted the binding energy of both C 1s and O 1s to higher field. The nanocomposite fibers showed higher thermal stability than the pristine PMMA fibers especially for the higher polymer concentrations, which is demonstrated from the TGA analysis. This improved thermal stability favors retaining the structural integrity of the materials when served as tissue scaffold. Both pristine PMMA and PMMA/QDs solutions showed a non-Newtonian behavior, while the electrospun fibers for both pristine and the nanocomposite demonstrated a pseudoplastic nature. Our preliminary data on the CHO cell culture study in the presence of PMMA-QDs nanocomposite fibers proved that the PMMA-QDs nanocomposite fibers have good biocompatibility with the CHO cells from the adhesion, viability and proliferation characteristics of the cell, while the sharp fluorescence signal from the fiber provided additional visual advantage toward future bioapplications.

Acknowledgments

This project is supported by the National Science Foundation – Chemical and Biological Separations (CBS) under the Eager Program (CBET 11-37441) managed by Dr. Rosemarie D. Wesson. S. Wei acknowledges the research start-up fund from Lamar University. The Welch foundation (V-0004) was also acknowledged.

References

[1] Witek MA, Wei S, Vaidya B, Adams AA, Zhu L, Stryjewski W, et al. Lab Chip 2004;4:464–72.
[2] Soper SA, Ford SM, Qi S, McCarley RL, Kelly K, Murphy MC. Anal Chem 2000; 72:642 A–51 A.
[3] McCarley RL, Vaidya B, Wei S, Smith AF, Patel AB, Feng J, et al. J Am Chem Soc 2005;127:842–3.
[4] Peppas NA, Langer R. Science 1994;263:1715–20.
[5] Marchant RE, Wang I. In: Greco RS, editor. Implantation biology: the host response and biomedical devices. CRC Press; 1994. p. 13–38.
[6] Guelcher SA, Srinivasan A, Dumas JE, Didier JE, McBride S, Hollinger JO. Biomaterials 2008;29:1762–75.
[7] Boger A, Wheeler K, Montali A, Gruskin E. J Biomed Mater Res B Appl Biomater 2009;90:760–6.
[8] Guo Z, Henry LL, Palshin V, Podlaha EJ. J Mater Chem 2006;16:1772–7.
[9] Ge J, Lei J, Zare RN. Nano Lett 2011;11:2551–4.
[10] Uyar T, Balan A, Toppare L, Besenbacher F. Polymer 2009;50:475–80.
[11] Uyar T, Nur Y, Hacaloglu J, Besenbacher F. Nanotechnology 2009;20: 125703–12.
[12] Osorio RA, Follmer M, Layne RW, Boucher RP, Talmadge KD, Basista JJ. US Pat; 2001:6726691.
[13] Murcia MJ, Shaw DL, Long EC, Naumann CA. Opt Commun 2008;281:1771–80.
[14] Reneker DH, Chun I. Nanotechnology 1996;7:216–23.
[15] Greiner A, Wendorff JH. Angew Chem Int Ed 2007;46:5670–3.
[16] Frenot A, Chronakis IS. Curr Opin Colloid Interface Sci 2003;8:64–75.
[17] Theron SA, Zussman E, Yarin AL. Polymer 2004;45:2017–30.
[18] Lin S, Cai Q, Ji J, Sui G, Yu Y, Yang X, et al. Compos Sci Technol 2008;68: 3322–9.
[19] Park S, Chase GG, Jeong K, Kim H. J Sol-Gel Sci Techn 2010;54:188–94.
[20] Sekak KA, Lowe A. J Am Ceram Soc 2011;94:611–9.
[21] Zhu J, Wei S, Rutman D, Haldolaarachchige N, Young DP, Guo Z. Polymer 2011; 52:2947–55.
[22] Zhu J, Wei S, Patil R, Rutman D, Kucknoor AS, Wang A, Guo Z. Polymer 2011; 52:1954–62.
[23] Chen X, Wei S, Gunesoglu C, Zhu J, Southworth CS, Sun L, et al. Macromol Chem Phys 2010;211:1775–83.
[24] Huang ZM, Zhang YZ, Kotaki M, Ramakrishna SA. Compos Sci Technol 2003; 63:2223–53.
[25] Ding W, Wei S, Zhu J, Chen X, Rutman D, Guo Z. Macromol Mater Eng 2010; 295:958–65.
[26] Li D, McCann J, Xia Y. J Am Ceram Soc 2006;89:1861–9.
[27] Ramaseshan R, Sundarrajan S, Jose R, Ramakrishna S. J Appl Phys 2007;102: 111101.
[28] Li WJ, Laurencin CT, Caterson EJ, Tuan RS, Ko FK. J Biomed Mater Res 2002;60: 613–21.

[29] Liu Y, Ji Y, Ghosh K, Clark RAF, Huang L, Rafailovich MH. J Biomed Mater Res Part A 2009;90A:1092–106.
[30] Alessandro P, Stefano P, Ripalta S, Giuseppe SN, Leonarda R, Clelia Prattichizzo LG, et al. Soft Matter 2010;6:1668–74.
[31] Chen S, Hou H, Harnisch F, Patil SA, Carmona-Martinez AA, Agarwal S, et al. Energy Environ Sci 2011;4:1417–21.
[32] Molla S, Compan V. J Membr Sci 2011;372:191–200.
[33] Dong Z, Kennedy SJ, Wu Y. J Power Sources 2011;196:4886–904.
[34] Ki-Joon J, Hoi Ri M, Ruminski AM, Jiang B, Kisielowski C, Bardhan R, Urban JJ. Nat Mater 2011;10:286–90.
[35] Ding B, Wang M, Yu J, Sun G. Sensors 2009;9:1609–24.
[36] Khang G, Jeong BJ, Lee HB, Park JB. Biomed Mater Eng 1995;5:259–73.
[37] Ribeiro DA, Sugui MM, Matsumoto MA, Duarte MA, Marques ME, Salvadori D. Oral Surg Oral Med Oral Pathol Oral Radiol Endod 2006;101(2):258–61.
[38] Ramakrishna S, Fujihara K, Teo W, Lim T and Ma Z. World Scientific Publishing Co. Pte. Ltd. 2005.
[39] Megelski S, Stephens JS, Chase DB, Rabolt JF. Macromolecules 2002;35: 8456–66.
[40] Socrates G. Infrared and raman characteristic group frequencies. 3rd ed. Chichester: John Wiley & Sons; 2001.
[41] Costache MC, Wang D, Heidecker MJ, Manias E, Wilkie CA. Polym for Adv Technologies 2006;17:272–80.
[42] Chen X, Wei S, Atarsingh Y, Patil R, Zhu J, Ximenes R, et al. Macromol Mater Eng 2011;296:434–43.
[43] Monakhova TV, Nedorezova PM, Bogayevskaya TA, Tsvetkova VI, Shlyapnikov YA. Polym Sci USSR 1988;30:2589–94.
[44] Chatterjee A, Deopura BL. J Appl Polym Sci 2006;100:3574–8.
[45] Troitskii BB, Troitskaya LS, Yakhnov AS, Lopatin MA, Novikova MA. Eur Polym J 1997;33:1587.
[46] Kelen T. Polymer degradation. New York: Van Nostrand-Reinhold; 1983.
[47] Rao MA. Rheology of fluid and semisolid foods: principles and applications. 2nd ed. New York: Springer; 2007.
[48] Schramm LL. Emulsions, foams, and suspensions: fundamentals and applications. Weinheim, Germany: Wiley VCH; 2005.
[49] Zhu J, Wei S, Ryu J, Budhathoki M, Liang G, Guo Z. J Mater Chem 2010;20: 4937–48.